Generalized Material Models in TLM—Part I: Materials with Frequency-Dependent Properties

John Paul, Christos Christopoulos, and David W. P. Thomas, *Member, IEEE*

***Abstract*—This paper presents the fundamentals of a unified approach for the treatment of general material properties in time-domain simulation based on transmission-line modeling (TLM). Linear frequency-dependent isotropic materials are dealt with in the first instance. The iteration schemes for one-dimensional (1-D) and three-dimensional (3-D) models are developed from Maxwell's curl equations and the constitutive relations. Results are presented showing the accuracy of this approach. In a companion paper, the approach is extended to the treatment of anisotropic materials.**

***Index Terms*—Anisotropic materials, frequency-dependent materials, nonhomogeneous media, time-domain electromagnetics, transmission-line modeling.**

I. Introduction

ALONG with the finite-difference time-domain (FDTD) method [1], [2], transmission-line modeling (TLM) [3], [4] is a differential time-domain method for the simulation of electromagnetic wave propagation. However, in FDTD, the electric and magnetic fields are separated in space and time by half a space-step and half a time-step respectively, whereas in TLM, all fields are solved at the same point in space (i.e., at the center of the cell) and at the same time. For description of propagation in complex materials such as those with anisotropic material tensors or displaying magnetoelectric coupling [5] in which it is necessary to solve the fields simultaneously, TLM offers a more straightforward solution than FDTD. As an introduction to this technique, in this paper, the TLM algorithms for one-dimensional (1-D) and three-dimensional (3-D) models involving linear frequency-dependent isotropic dielectric media are developed from Maxwell's equations and the constitutive relations. In a companion paper [6], the more general formulation to include the modeling of anisotropic materials is described. It is shown that TLM leads to a more efficient formulation for anisotropic problems when compared with FDTD. The method developed here is based on that of de Menezes and Hoefer [7]. However, the present method based on $\mathcal{Z}$ transforms is more efficient and offers a systematic approach to the treatment of all material properties including anisotropy, magnetoelectric coupling, and nonlinearities. $\mathcal{Z}$-transform methods have been utilized by Sullivan for the development of iteration procedures in FDTD [8]–[10] and extended to more general media by Weedon [11]. Applying this approach to TLM, in this paper, $\mathcal{Z}$ transforms are used to develop models of frequency-dependent dielectric material response. To correlate with previous studies reported in the literature, the formulation is validated using three examples that have been previously studied in FDTD. First, the plasma slab of Luebbers [12] is modeled in TLM using a frequency-dependent conductivity rather than the permittivity approach used in FDTD. Second, as an example of a first-order dielectric material, the reflection coefficient of Luebbers' air–water interface [13] is modeled. Finally, propagation in Kelley's second-order (Lorentz) dielectric [14] is studied. All numerical results gave close agreement with analysis.

Manuscript received July 21, 1999. This work was supported by the Engineering and Physical Sciences Research Council, U.K., and the National Physical Laboratory, U.K., through the funding of a studentship.

The authors are with the Electromagnetics Research Group, School of Electrical and Electronic Engineering, University of Nottingham, University Park, Nottingham, NG7 2RD, U.K.

Publisher Item Identifier S 0018-926X(99)09846-4.

TABLE I
THE ELECTROMAGNETIC QUANTITIES

Quantity	*Symbol*	*Units*
Electric field	$\underline{E}$	V m^{-1}
Magnetic field	$\underline{H}$	A m^{-1}
Electric current density	$\underline{J}_e$	A m^{-2}
Magnetic voltage density	$\underline{J}_m$	V m^{-2}
Electric flux density	$\underline{D}$	C m^{-2}
Magnetic flux density	$\underline{B}$	Wb m^{-2}
Free electric current density	$\underline{J}_{ef}$	A m^{-2}
Free magnetic voltage density	$\underline{J}_{mf}$	V m^{-2}
Electric conductivity	σ_e	S m^{-1}
Magnetic resistivity	σ_m	Ω m^{-1}
Electric susceptibility	χ_e	
Magnetic susceptibility	χ_m	
Free-space permittivity	ε_0	F m^{-1}
Free-space permeability	μ_0	H m^{-1}

II. Formulation

A. Maxwell's Equations and the Constitutive Relations

The TLM formulation is developed from Maxwell's curl equations and the constitutive relations [5]. Equation (1) expresses Maxwell's curl equations in compact form

$$\begin{bmatrix} \nabla \times \underline{H} \\ -\nabla \times \underline{E} \end{bmatrix} = \begin{bmatrix} \underline{J}_e \\ \underline{J}_m \end{bmatrix} + \frac{\partial}{\partial t} \begin{bmatrix} \underline{D} \\ \underline{B} \end{bmatrix}. \tag{1}$$

The electromagnetic quantities are defined in Table I.

The constitutive relations for the current and voltage densities are expressed in (2). In this equation, $*$ denotes a time-domain convolution operation

$$\begin{bmatrix} \underline{J}_e \\ \underline{J}_m \end{bmatrix} = \begin{bmatrix} \underline{J}_{ef} + \sigma_e * \underline{E} \\ \underline{J}_{mf} + \sigma_m * \underline{H} \end{bmatrix}. \tag{2}$$

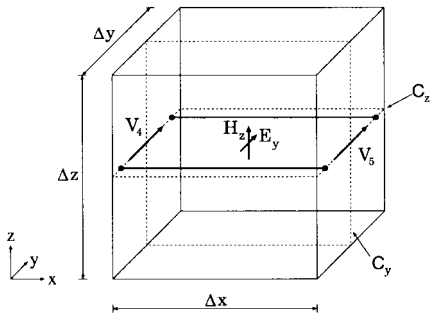

Fig. 1. One-dimensional TLM node describing propagation in x.

Equation (3) expresses the constitutive relations for the flux densities. In the general case, the material parameters of the constitutive relations describe causal time functions

$$\begin{bmatrix} \underline{D} \\ \underline{B} \end{bmatrix} = \begin{bmatrix} \varepsilon_0 \underline{E} + \varepsilon_0 \chi_e * \underline{E} \\ \mu_0 \underline{H} + \mu_0 \chi_m * \underline{H} \end{bmatrix}. \tag{3}$$

Substitution of (2) and (3) into (1) yields

$$\begin{bmatrix} \nabla \times \underline{H} \\ -\nabla \times \underline{E} \end{bmatrix} - \begin{bmatrix} \underline{J}_{ef} \\ \underline{J}_{mf} \end{bmatrix} = \begin{bmatrix} \sigma_e * \underline{E} \\ \sigma_m * \underline{H} \end{bmatrix} + \frac{\partial}{\partial t} \begin{bmatrix} \varepsilon_0 \underline{E} + \varepsilon_0 \chi_e * \underline{E} \\ \mu_0 \underline{H} + \mu_0 \chi_m * \underline{H} \end{bmatrix}. \tag{4}$$

The time-domain model represents a discrete-time solution of (4), solving for the fields $\underline{E}$ and $\underline{H}$ at each time-step.

B. 1-D Formulation

In order to illustrate the physical basis of the models with the minimum of mathematical complexity, the development of a 1-D formulation is first described. This sets the scene for the full 3-D formulation presented in the next section. Considering propagation in x with the electric field polarized in y and the magnetic field polarized in z, Fig. 1 shows the 1-D model: This node has two ports (V_4 and V_5) and two total field quantities (E_y and H_z) evaluated at the center of the cell. The curl operations are solved using the integration contours $\mathcal{C}_y$ and $\mathcal{C}_z$. For consistency with the 3-D development, the port numbers are from the 3-D node to be discussed in Section II-C.

Reduction of (4) to describe this simple case gives

$$-\frac{\partial}{\partial x} \begin{bmatrix} H_z \\ E_y \end{bmatrix} - \begin{bmatrix} J_{efy} \\ J_{mfz} \end{bmatrix} = \begin{bmatrix} \sigma_e * E_y \\ \sigma_m * H_z \end{bmatrix} + \frac{\partial}{\partial t} \begin{bmatrix} \varepsilon_0 E_y + \varepsilon_0 \chi_e * E_y \\ \mu_0 H_z + \mu_0 \chi_m * H_z \end{bmatrix}. \tag{5}$$

Using regular space-steps $\Delta x = \Delta y = \Delta z = \Delta \ell$ and η_0 as the intrinsic impedance of free-space, the transmission-line model of (5) is found by application of the field-circuit equivalences [4]

$$\begin{aligned} E_y &= -V_y/\Delta\ell \quad H_z = -i_z/(\Delta\ell\,\eta_0) \\ J_{efy} &= -i_{fy}/(\Delta\ell^2\,\eta_0) \quad J_{mfz} = -V_{fz}/\Delta\ell^2 \\ \sigma_e &= g_e/(\Delta\ell\,\eta_0) \quad \sigma_m = r_m\eta_0/\Delta\ell. \end{aligned} \tag{6}$$

Because we are dealing with linear materials, by applying the Laplace transform the time-domain convolutions in (5) are converted to frequency-domain multiplications and the time derivative is transformed using $\partial/\partial t \rightarrow s = \overline{s}/\Delta t$ where Δt is the time-step. The spatial derivative is normalized using $\partial/\partial x \rightarrow (1/\Delta\ell)\partial/\partial\overline{x}$ and speed of propagation in the 1-D model is the speed of light in free-space, $\Delta\ell/\Delta t = c$ [4]. Applying these transformations to (5) leads to

$$-\frac{\partial}{\partial \overline{x}} \begin{bmatrix} i_z \\ V_y \end{bmatrix} - \begin{bmatrix} i_{fy} \\ V_{fz} \end{bmatrix} = \begin{bmatrix} g_e V_y \\ r_m i_z \end{bmatrix} + \overline{s} \begin{bmatrix} V_y + \chi_e V_y \\ i_z + \chi_m i_z \end{bmatrix}. \tag{7}$$

By application of Stokes' theorem using the integration contours $\mathcal{C}_y$ and $\mathcal{C}_z$ indicated in Fig. 1, (7) becomes

$$\begin{bmatrix} V_4 + V_5 \\ V_4 - V_5 \end{bmatrix} - \begin{bmatrix} i_{fy} \\ V_{fz} \end{bmatrix} = \begin{bmatrix} g_e V_y \\ r_m i_z \end{bmatrix} + \overline{s} \begin{bmatrix} V_y + \chi_e V_y \\ i_z \chi_m i_z \end{bmatrix}. \tag{8}$$

Converting to the traveling wave format and using superscript i to denote incident wave quantities, (8) becomes

$$2\begin{bmatrix} V_4 + V_5 \\ V_4 - V_5 \end{bmatrix}^i - \begin{bmatrix} i_{fy} \\ V_{fz} \end{bmatrix} = 2\begin{bmatrix} V_y \\ i_z \end{bmatrix} + \begin{bmatrix} g_e V_y \\ r_m i_z \end{bmatrix} + \overline{s} \begin{bmatrix} \chi_e V_y \\ \chi_m i_z \end{bmatrix}. \tag{9}$$

The left-hand side (LHS) of (9) is the external excitation of the node consisting of the traveling voltage pulses incident on the node and any free-source excitation. Defining the LHS of (9) as the reflected fields[1] and using superscript r to denote reflected wave quantities, (9) is

$$2\begin{bmatrix} V_y \\ -i_z \end{bmatrix}^r = 2\begin{bmatrix} V_y \\ i_z \end{bmatrix} + \begin{bmatrix} g_e V_y \\ r_m i_z \end{bmatrix} + \overline{s} \begin{bmatrix} \chi_e V_y \\ \chi_m i_z \end{bmatrix}. \tag{10}$$

Defining transmission coefficients $t_{ey} = 2/(2 + g_e + \overline{s}\,\chi_e)$ and $t_{mz} = 2/(2 + r_m + \overline{s}\,\chi_m)$, (10) becomes

$$\begin{bmatrix} V_y \\ i_z \end{bmatrix} = \begin{bmatrix} t_{ey} & \\ & t_{mz} \end{bmatrix} \cdot \begin{bmatrix} V_y \\ -i_z \end{bmatrix}^r. \tag{11}$$

The solution of (11) for various materials is detailed in Section III. Assuming we have calculated the total fields V_y and i_z, the reflected voltage pulses on the transmission-lines now need to be evaluated. The first diagram in Fig. 2

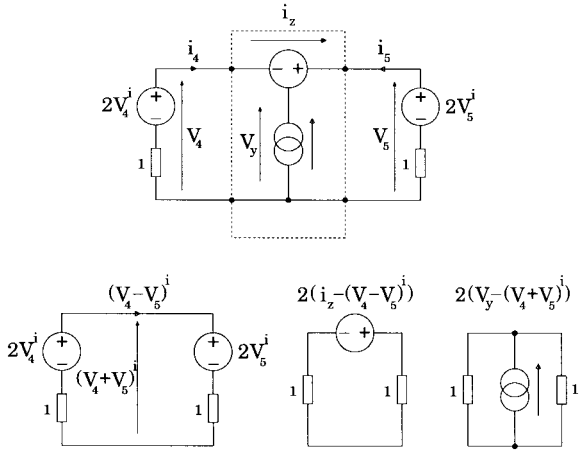

Fig. 2. Development of the 1-D node.

[1] These quantities are defined as reflected to correlate with previous formulations in the literature [7], [15] in which these are the voltages reflected into the infinitesimal stub connecting the link-lines and the load. In this formulation, these quantities are called the reflected *fields* to distinguish them from the reflected *voltages* on the transmission lines.

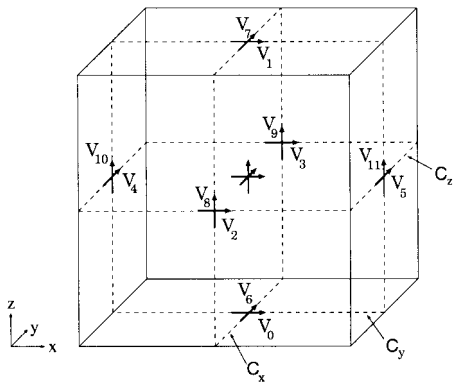

Fig. 3. Three-dimensional node.

shows the equivalent circuit of the 1-D node. This network is decomposed into the three circuits shown. The currents i_4 and i_5 flowing in the transmission lines are found by superposition of the three circuits, i.e.

$$i_4 = -V_y + i_z + V_4^i + V_5^i, \quad i_5 = -V_y - i_z + V_4^i + V_5^i. \tag{12}$$

The total voltages on the transmission lines are

$$V_4 = 2V_4^i - i_4, \quad V_5 = 2V_5^i - i_5. \tag{13}$$

The reflected voltages are obtained from

$$V_4^r = V_4 - V_4^i, \quad V_5^r = V_5 - V_5^i. \tag{14}$$

By substitution of (12) and (13) into (14), the reflected voltages are obtained as a function of the incident voltages and the total fields

$$V_4^r = V_y - i_z - V_5^i, \quad V_5^r = V_y + i_z - V_4^i. \tag{15}$$

In summary, the field update process is split into three steps. First, the reflected fields are calculated from the incident voltages and free-sources using (10). Next, the total fields are evaluated using (11). Finally, the reflected transmission-line voltages are obtained using (15) The algorithm is completed by the connection process in which the reflected voltages are swapped between nodes to become the incident voltages of the next time step [4].

C. 3-D Formulation The formulation of the 3-D TLM method based on the symmetrical condensed node (SCN) [16] is developed by extension of the 1-D model discussed in the previous section. The 3-D cell is shown in Fig. 3.

The node has 12 ports, $(V_0 \cdots V_{11})$, and six total field quantities $(E_x, E_y, E_z, H_x, H_y,$ and $H_z)$ at the center of the cell. The external excitation of the 3-D node is

$$2\begin{bmatrix} (V_0+V_1+V_2+V_3) \\ (V_4+V_5+V_6+V_7) \\ (V_8+V_9+V_{10}+V_{11}) \\ -(V_6-V_7-V_8+V_9) \\ -(V_{10}-V_{11}-V_0+V_1) \\ -(V_2-V_3-V_4+V_5) \end{bmatrix}^i - \begin{bmatrix} i_{fx} \\ i_{fy} \\ i_{fz} \\ V_{fx} \\ V_{fy} \\ V_{fz} \end{bmatrix} \equiv 2\begin{bmatrix} V_x \\ V_y \\ V_z \\ -i_x \\ -i_y \\ -i_z \end{bmatrix}^r. \tag{16}$$

Defining the matrix $\underline{\underline{R}}_1^T$, the vector of incident voltages $\underline{V}^i$, the vector of free-sources $\underline{V}_f$ and the vector of reflected fields

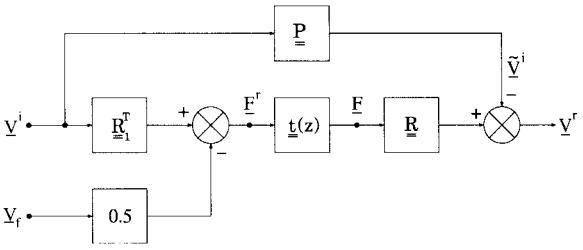

Fig. 4. Signal flow graph of the TLM process.

$\underline{F}^r$, (16) can be written compactly as

$$2\underline{\underline{R}}_1^T \cdot \underline{V}^i - \underline{V}_f = 2\,\underline{F}^r. \tag{17}$$

Because the speed of propagation in the 3-D model is $\Delta\ell/\Delta t = 2c$ [4], the transmission coefficients are $t_{ey} = 2/(4 + g_e + \overline{s}\,2\chi_e)$ and $t_{mz} = 2/(4 + r_m + \overline{s}\,2\chi_m)$. The 3-D equivalent of (11) is

$$\begin{bmatrix} V_x \\ V_y \\ V_z \\ i_x \\ i_y \\ i_z \end{bmatrix} = \begin{bmatrix} t_{ex} & & & & & \\ & t_{ey} & & & & \\ & & t_{ez} & & & \\ & & & t_{mx} & & \\ & & & & t_{my} & \\ & & & & & t_{mz} \end{bmatrix} \cdot \begin{bmatrix} V_x \\ V_y \\ V_z \\ -i_x \\ -i_y \\ -i_z \end{bmatrix}^r. \tag{18}$$

Writing the vector of total fields as $\underline{F}$ and the matrix of transmission coefficients as $\underline{\underline{t}}$, (18) is written compactly as

$$\underline{F} = \underline{\underline{t}} \cdot \underline{F}^r. \tag{19}$$

As in the 1-D example, the reflected voltages on the transmission-lines are required. Extending (15) to the 3-D model yields

$$\begin{bmatrix} V_0 \\ V_1 \\ V_2 \\ V_3 \\ V_4 \\ V_5 \\ V_6 \\ V_7 \\ V_8 \\ V_9 \\ V_{10} \\ V_{11} \end{bmatrix}^r = \begin{bmatrix} V_x - i_y - V_1^i \\ V_x + i_y - V_0^i \\ V_x + i_z - V_3^i \\ V_x - i_z - V_2^i \\ V_y - i_z - V_5^i \\ V_y + i_z - V_4^i \\ V_y + i_x - V_7^i \\ V_y - i_x - V_6^i \\ V_z - i_x - V_9^i \\ V_z + i_x - V_8^i \\ V_z + i_y - V_{11}^i \\ V_z - i_y - V_{10}^i \end{bmatrix}. \tag{20}$$

Writing the vector of reflected voltages as $\underline{V}^r$ and defining the matrices $\underline{\underline{R}}$ and $\underline{\underline{P}}$, (18) in concise form is

$$\underline{V}^r = \underline{\underline{R}} \cdot \underline{F} - \underline{\underline{P}} \cdot \underline{V}^i = \underline{\underline{R}} \cdot \underline{F} - \tilde{\underline{V}}^i \tag{21}$$

where $\tilde{\underline{V}}^i$ is the vector of voltages incident on the lines opposite those used to obtain $\underline{V}^i$. Thus, the iteration process in the 3-D method is simply an extended form of that previously developed for the 1-D model. The process is summarized as the flow diagram of Fig. 4.

For the modeling of general materials, only the transmission block $\underline{\underline{t}}(z)$ of Fig. 4 needs to be modified. The argument

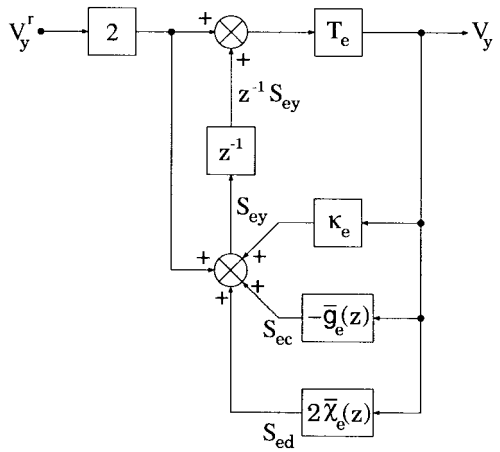

Fig. 5. Electric field update process in a dielectric material.

z is the time-shift operator and emphasizes the frequency-dependent response of this block. The development of $\underline{\underline{t}}(z)$ for description of frequency-dependent material behavior in the time-domain is detailed in the next section.

III. Frequency-Dependent Materials

In this section, the method for the inclusion of frequency-dependent material properties in TLM is presented.

A. General Isotropic Materials

For clarity, models of dielectric responses in nonmagnetic materials are developed. Because there are no magnetic effects, the transmission coefficient t_{mz} of (11) is unity, thus, in all cases studied below, the total magnetic field is found using $i_z = -i_z^r$. Reduction of (10) to describe the dielectric case and applying the bilinear transform $\overline{s} \rightarrow 2(1-z^{-1})/(1+z^{-1})$ gives

$$2V_y^r = 2V_y + g_e(z)V_y + 2\left(\frac{1-z^{-1}}{1+z^{-1}}\right)\chi_e(z)V_y. \tag{22}$$

As detailed for particular materials in the next sections, for the time-domain modeling of causal material functions, the frequency dependence can always be shifted to become a function of the field value at the previous time-step by taking partial fraction expansions such as

$$(1+z^{-1})g_e(z) = g_{e0} + z^{-1}(g_{e1} + \overline{g}_e(z)) \tag{23}$$

$$(1-z^{-1})\chi_e(z) = \chi_{e0} - z^{-1}(\chi_{e1} + \overline{\chi}_e(z)). \tag{24}$$

Substitution of (23) and (24) in (22) and manipulating leads to

$$V_y = T_e(2V_y^r + z^{-1}S_{ey}) \tag{25}$$

where the coefficient $T_e = (2 + g_{e0} + 2\chi_{e0})^{-1}$ and the main accumulator S_{ey} is

$$S_{ey} = 2V_y^r + \kappa_e V_y - \overline{g}_e(z)V_y + 2\overline{\chi}_e(z)V_y. \tag{26}$$

In (26), the coefficient $\kappa_e = -(2 + g_{e1} - 2\chi_{e1})$. The process described by (25) and (26) is illustrated as the flow graph of Fig. 5. This is the block $\underline{\underline{t}}(z)$ in Fig. 4 for this particular case. In the next section, the block $-\overline{g}_e(z)$ is developed for the modeling of an unmagnetized plasma.

B. Unmagnetized Plasma

The frequency-domain electric conductivity of an unmagnetized plasma with collisions is described by a first-order conductivity term

$$\sigma_e(s) = \frac{\sigma_{e0}}{1 + s\tau_c}. \tag{27}$$

In (27), τ_c is the collision time and the static electric conductivity $\sigma_{e0} = N_0 q^2 \tau_c / m = \omega_p^2 \varepsilon_0 \tau_c$ where N_0 is the electron density (m^{-3}), q is the electron charge, m is the electron mass, and ω_p is the plasma frequency. Using normalized conductance $g_{ec} = \sigma_{e0}\Delta\ell\eta_0$ and transforming to the $\mathcal{Z}$-domain using the impulse invariant method, (27) becomes

$$g_e(z) = \frac{g_{ec}(1-\beta_c)}{1 - z^{-1}\beta_c} \tag{28}$$

where $\beta_c = e^{-\Delta t/\tau_c}$. As described in the previous section, the model follows from the partial fraction expansion of (23) leading to

$$(1+z^{-1})g_e(z) = g_{ec}(1-\beta_c) + z^{-1}\frac{g_{ec}(1-\beta_c^2)}{1 - z^{-1}\beta_c}. \tag{29}$$

Comparison of (23) and (29) gives the coefficients $g_{e0} = g_{ec}(1-\beta_c)$ and $g_{e1} = 0$, with the frequency-dependent function $\overline{g}_e(z) = \alpha_c/(1 - z^{-1}\beta_c)$ where $\alpha_c = g_{ec}(1-\beta_c^2)$. Thus, the electric field update scheme in a TLM model of propagation in an unmagnetized plasma with a frequency-independent background susceptibility of $\chi_{e\infty}$ is given by (25) and (26), modified with a conductive material accumulator S_{ec}. The process is

$$V_y = T_e(2V_y^r + z^{-1}S_{ey}) \tag{30}$$

$$S_{ec} = -\alpha_c V_y + z^{-1}\beta_c S_{ec} \tag{31}$$

$$S_{ey} = 2V_y^r + \kappa_e V_y + S_{ec} \tag{32}$$

where $T_e = (2 + g_{e0} + 2\chi_{e\infty})^{-1}$ and $\kappa_e = -(2 - 2\chi_{e\infty})$. Once the total fields V_y and i_z and the new values of the accumulators S_{ec} and S_{ey} have been evaluated, the reflected voltages on the transmission lines are obtained using (15).

Using this technique, the model of an unmagnetized plasma requires two backstores for each electric field component. The next section details the formulation of the block $2\overline{\chi}_e(z)$ for the modeling of first-order dielectric media.

C. Debye Dielectric

The frequency-domain electric susceptibility of a first-order (Debye) dielectric is

$$\chi_e(s) = \chi_{e\infty} + \frac{\Delta\chi_e}{1 + s\tau_e} \tag{33}$$

where $\chi_{e\infty}$ is the optical susceptibility, $\Delta\chi_e$ is the susceptibility contrast of the dispersion, and τ_e is the dielectric relaxation time. As for the plasma model, transforming to the $\mathcal{Z}$ domain using $\beta_e = e^{-\Delta t/\tau_e}$ yields

$$\chi_e(z) = \chi_{e\infty} + \frac{\Delta\chi_e(1-\beta_e)}{1 - z^{-1}\beta_e}. \tag{34}$$

The partial fraction expansion shown in (24) leads to the coefficients

$$\chi_{e0} = \chi_{e\infty} + \Delta\chi_e(1-\beta_e), \chi_{e1} = \chi_{e\infty} \tag{35}$$

and the frequency-dependent function

$$\overline{\chi}_e(z) = \frac{\alpha_e/2}{1 - z^{-1}\beta_e} \tag{36}$$

where $\alpha_e/2 = \Delta\chi_e(1-\beta_e)^2$. The update scheme for the electric field in a Debye dielectric with a frequency-independent normalized conductivity g_e is given by (25) and (26), modified with a dielectric material accumulator S_{ed}, i.e.

$$V_y = T_e(2V_y^r + z^{-1}S_{ey}) \tag{37}$$

$$S_{ed} = \alpha_e V_y + z^{-1}\beta_e S_{ed} \tag{38}$$

$$S_{ey} = 2V_y^r + \kappa_e V_y + S_{ed} \tag{39}$$

where $T_e = (2 + g_e + 2\chi_{e0})^{-1}$ and $\kappa_e = -(2 + g_e - 2\chi_{e1})$.

As for the plasma model, the algorithm describing a Debye dielectric requires two backstores per electric field component.

D. Lorentz Dielectric

The frequency-domain electric susceptibility of a second-order (Lorentz) dielectric is

$$\chi_e(s) = \chi_{e\infty} + \frac{\Delta\chi_e\omega_0^2}{s^2 + s2\delta + \omega_0^2} \tag{40}$$

where δ is the damping frequency and ω_0 is the resonant frequency. Transforming (40) to the $\mathcal{Z}$ domain gives

$$\chi_e(z) = \chi_{e\infty} + \frac{\Delta\chi_e(1 - 2A_e + A_e^2 + B_e^2)z^{-1}}{1 - z^{-1}2A_e + z^{-2}(A_e^2 + B_e^2)} \tag{41}$$

where using $\beta = \sqrt{\omega_0^2 - \delta^2}$, $A_e = e^{-\delta\Delta t}\cos(\beta\Delta t)$ and $B_e = e^{-\delta\Delta t}\sin(\beta\Delta t)$. Defining coefficients $a_1 = 2A_e$, $a_2 = -(A_e^2 + B_e^2)$, and $K_1 = \Delta\chi_e(1 - 2A_e + A_e^2 + B_e^2)$, (41) becomes

$$\chi_e(z) = \chi_{e\infty} + \frac{K_1 z^{-1}}{1 - z^{-1}a_1 - z^{-2}a_2}. \tag{42}$$

Because of the z^{-1} term in the numerator of the frequency-dependent part of (42), there is no need to take a partial fraction expansion to shift the frequency-dependent function to the previous time-step. The coefficients of (24) are $\chi_{e0} = \chi_{e1} = \chi_{e\infty}$ and the frequency-dependent function is

$$\overline{\chi}_e(z) = \frac{b_1'/2 + z^{-1}b_2'/2}{1 - z^{-1}a_1 - z^{-2}a_2} \tag{43}$$

where the coefficients are $b_1' = -2K_1$ and $b_2' = 2K_1$. The model is similar to the first-order dielectric, with the dielectric material accumulator modified to

$$S_{ed} = \left[\frac{b_1' + z^{-1}b_2'}{1 - z^{-1}a_1 - z^{-2}a_2}\right]V_y. \tag{44}$$

An efficient method for the evaluation of this function is the phase-variable state-space form [17]. Defining state variables

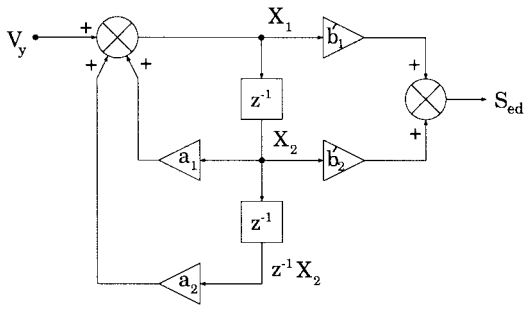

Fig. 6. Phase-variable description of Lorentz media.

X_1 and X_2, the discrete state-space and output equations are

$$\begin{bmatrix} X_1 \\ X_2 \end{bmatrix} = z^{-1}\begin{bmatrix} a_1 & a_2 \\ 1 & \end{bmatrix} \cdot \begin{bmatrix} X_1 \\ X_2 \end{bmatrix} + \begin{bmatrix} 1 \\ 0 \end{bmatrix} V_y \tag{45}$$

$$S_{ed} = \begin{bmatrix} b_1' & b_2' \end{bmatrix} \cdot \begin{bmatrix} X_1 \\ X_2 \end{bmatrix}. \tag{46}$$

The update scheme for the electric field in a Lorentz dielectric is

$$V_y = T_e(2V_y^r + z^{-1}S_{ey}) \tag{47}$$

$$X_1 = z^{-1}a_1X_1 + z^{-1}a_2X_2 + V_y \tag{48}$$

$$X_2 = z^{-1}X_1 \tag{49}$$

$$S_{ey} = 2V_y^r + \kappa_e V_y + b_1'X_1 + b_2'X_2 \tag{50}$$

where $T_e = (2 + g_e + 2\chi_{e0})^{-1}$ and $\kappa_e = -(2 + g_e - 2\chi_{e1})$.

Thus, the present method for modeling Lorentz materials requires three backstores per electric field component. The flow diagram illustrating the discrete state-space system is shown in Fig. 6. This system is the block $2\overline{\chi}_e(z)$ of Fig. 5 for modeling a Lorentz dielectric.

IV. Results

In this section, results for propagation in three types of frequency-dependent materials are presented.

A. Plasma Slab

The reflection coefficient of the plasma slab originally studied in FDTD [12] was calculated using TLM. The material parameters were $\omega_p = 2\pi \times 28.7 \times 10^9$, $\tau_c = 50 \times 10^{-12}$ s, and $\chi_{e\infty} = 0$. The space-step was chosen as $\Delta\ell = 75$ μm and the total length of the problem space in x was 800 cells with the plasma slab having thickness 1.5 cm. In the 3-D model, the cross-section in y and z was 2 $\times$ 2 cells. The calculated reflection coefficient of the slab for both 1-D and 3-D cases shows agreement with the analytic solution obtained from classical boundary matching methods [5] in Fig. 7. As noted in [12], it was necessary to run the FDTD simulations at half the free-space time-step (the Courant limit) in order to avoid instabilities. In the TLM discretization, the models were run at the free-space time step and no stability problems were encountered.

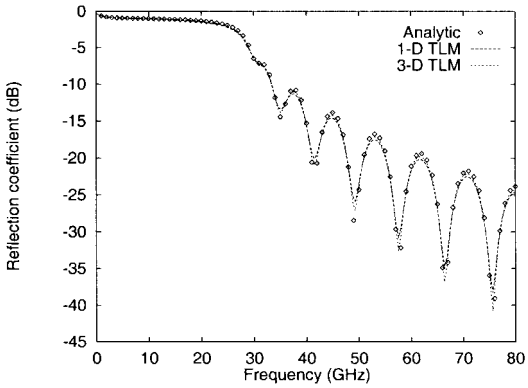

Fig. 7. Plasma slab: frequency-domain reflection coefficient.

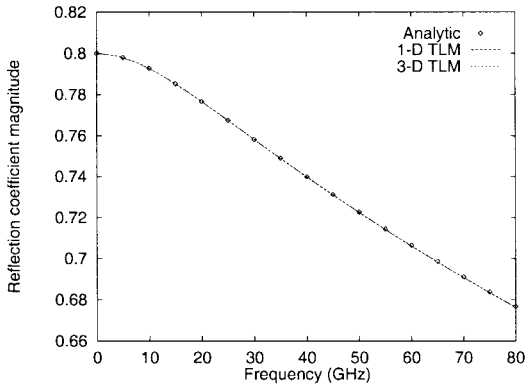

Fig. 8. Air–water interface: frequency-domain reflection coefficient.

B. Air–Water Interface

The technique was used to calculate the reflection coefficient of the air–water interface studied in [13]. The material parameters were $\chi_{e\infty} = 1.8$, $\Delta\chi_e = 79.2$, $\tau_e = 9.4 \times 10^{-12}$ s, and $g_e = 0$. The 1-D and 3-D models used 1000 nodes in x of space-step $\Delta\ell = 37.5$ μm. As in the previous example, the cross section of the 3-D model was two cells in both y and z. The calculated frequency-domain reflection coefficient is compared with the analytic solution in Fig. 8.

C. Air–Lorentz Material Interface

As an example of a second-order material, propagation in the Lorentz material of [14] was studied. The parameters were: $\chi_{e\infty} = 0.5$, $\Delta\chi_e = 1.5$, $\omega_0 = 2\pi \times 20 \times 10^9$, and $\delta = 0.1\omega_0$. The space-step was $\Delta\ell = 250$ μm, the problem space had 1000 cells in x, 50 of free-space, and 950 of Lorentz material. The 3-D domain had a cross section of 2×2 nodes. In Fig. 9, the calculated frequency-domain reflection coefficient of the interface shows close agreement with the analytic solution. Because of the smaller time-step used in 3-D, the 3-D model performs slightly better than the 1-D model at higher frequencies.

The electric field initial condition and distribution after 737.5 ps is shown in Fig. 10. In agreement with the results presented in [14]; a sinusoidal precursor is forming ahead of the main pulse. Careful examination of Fig. 10 at $x \sim 0.24$ m reveals that in the 3-D model, a small spurious pulse of a derivative Gaussian form is propagating at the speed of light through the Lorentz material.

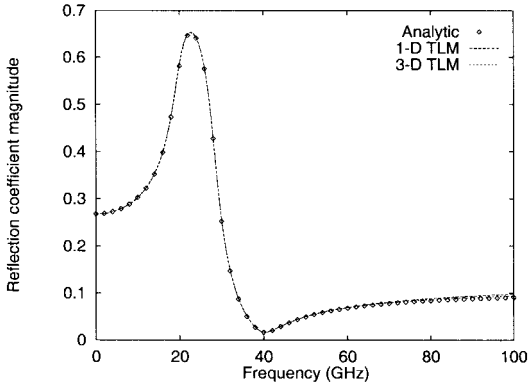

Fig. 9. Air–Lorentz material interface: frequency-domain reflection coefficient.

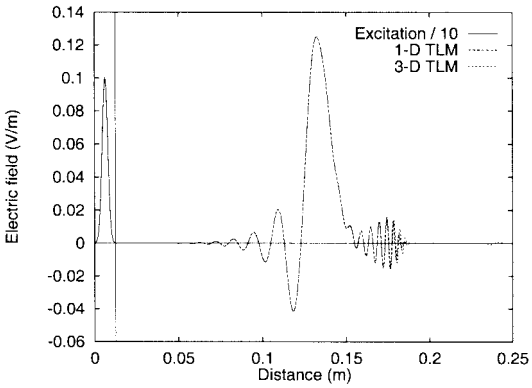

Fig. 10. Air–Lorentz material interface: electric field distribution after 737.5 ps.

V. Conclusion

In this paper, the iteration schemes for 1-D and 3-D TLM simulations of linear isotropic frequency-dependent materials were developed from Maxwell's equations and the constitutive relations. $\mathcal{Z}$-transform methods were used to incorporate frequency-dependent material properties into the TLM algorithm, leading to a formal technique applicable to all linear materials. Results have been presented that show that the method yields accurate results and suffers from no stability problems. Although this paper has concentrated on isotropic dielectrics, a unified approach has been introduced that can be extended to deal with very general material properties. In a companion paper, the case of materials with frequency-dependent anisotropic parameters is considered.

References

[1] K. S. Yee, "Numerical solution of initial boundary value problems involving Maxwell's equations in isotropic media," *IEEE Trans. Antennas Propagat.*, vol. AP-14, pp. 302–307, May 1966.

[2] A. Taflove, *Computational Electrodynamics: The Finite-Difference Time-Domain Method*. Norwood, MA: Artech House, 1995.

[3] P. B. Johns and R. L. Beurle, "Numerical solution of 2-dimensional scattering problems using a transmission-line matrix," *Proc. Inst. Elect. Eng.*, vol. 118, no. 9, pp. 1203–1208, Sept. 1971.

[4] C. Christopoulos, *The Transmission-Line Modeling Method: TLM*. Piscataway, NJ: IEEE Press, 1995.
[5] J. A. Kong, *Electromagnetic Wave Theory*. New York: Wiley, 1986.
[6] J. Paul, C. Christopoulos, and D. W. P. Thomas, "Generalized material models in TLM—Part 2: Materials with anisotropic properties," *IEEE Trans. Antennas Propagat.*, this issue, pp. 1535–1542.
[7] L. de Menezes and W. J. R. Hoefer, "Modeling of general constitutive relationships using SCN TLM," *IEEE Trans. Microwave Theory Tech.*, vol. 44, pp. 854–861, June 1996.
[8] D. M. Sullivan, "Frequency dependent FDTD methods using Z-transform," *IEEE Trans. Antennas Propagat.*, vol. 40, pp. 1223–1230, Oct. 1992.
[9] ——, "Nonlinear FDTD formulations using Z transforms," *IEEE Trans. Microwave Theory Tech.*, vol. 43, pp. 676–682, Mar. 1995.
[10] ——, "Z-transform theory and the FDTD method," *IEEE Trans. Antennas Propagat.*, vol. 44, pp. 28–34, Jan. 1996.
[11] W. H. Weedon and C. M. Rappaport, "A general method for FDTD modeling of wave propagation in arbitrary frequency-dispersive media," *IEEE Trans. Antennas Propagat.*, vol. 45, pp. 401–410, Mar. 1997.
[12] R. J. Luebbers, F. Hunsberger, and K. S. Kunz, "A frequency-dependent finite-difference time-domain formulation for transient propagation in plasma," *IEEE Trans. Antennas Propagat.*, vol. 39, pp. 29–34, Jan. 1991.
[13] R. Luebbers, F. Hunsberger, K. S. Kunz, R. B. Standler, and M. Schneider, "A frequency-dependent finite-difference time-domain formulation for dispersive materials," *IEEE Trans. Electromagn. Compat.*, vol. 32, pp. 222–227, Aug. 1990.
[14] D. F. Kelley and R. J. Luebbers, "Piecewise linear recursive convolution for dispersive media using FDTD," *IEEE Trans. Antennas Propagat.*, vol. 44, pp. 792–797, June 1996.
[15] P. Russer, P. P. M. So, and W. J. R. Hoefer, "Modeling of nonlinear active regions in TLM," *IEEE Microwave Guided Wave Lett.*, vol. 1, pp. 10–13, Jan. 1991.
[16] P. B. Johns, "A symmetrical condensed node for the TLM method," *IEEE Trans. Microwave Theory Tech.*, vol. 35, pp. 370–377, Apr. 1987.
[17] R. T. Stefani, C. J. Savant, B. Shahian, and G. H. Hostetter, *Design of Feedback Control Systems*. Orlando, FL: Saunders College Publ., 1994.

John Paul was born in Peterborough, U.K., in 1960. He received the M.Eng. and the Ph.D. degrees in electrical and electronic engineering from the University of Nottingham, U.K., in 1994 and 1999, respectively. His Ph.D. dissertation involved the application of signal processing and control system techniques to the modeling of general materials in time-domain TLM.

He is currently employed as a Research Associate with the Electromagnetics Research Group, University of Nottingham. His research interests are in the application of signal processing techniques to the modeling of complex electromagnetic systems, the design of novel electromagnetic wave absorbers, and the time-domain modeling of general wave phenomena.

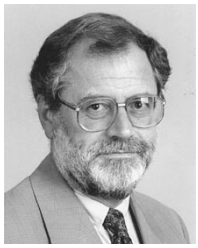

Christos Christopoulos was born in Patras, Greece, in 1946. He received the Diploma in electrical and mechanical engineering from the National Technical University of Athens, Greece, in 1969, and the M.Sc. and D.Phil. from the University of Sussex, U.K., in 1970 and 1975, respectively.

In 1974, he joined the Arc Research Project at the University of Liverpool, U.K., and spent two years working on vacuum arcs and breakdown while on attachment to the United Kingdom Atomic Energy Authority (UKAEA) Culham Laboratories. In 1976 he joined the University of Durham, U.K., as a Senior Demonstrator in electrical engineering science. In October 1978 he joined the Department of Electrical and Electronic Engineering, University of Nottingham, where he is now a Professor of electrical engineering. He has published five technical books. His research interests are in electrical discharges and plasmas, electromagnetic compatibility, electromagnetics, and protection and simulation of power networks.

Dr. Christopoulos received the Institute of Electrical Engineers Snell Premium and Institute of Electrical Engineers Electronics Letters Premium Awards in 1995.

David W. P. Thomas (M'95) was born in Padstow, U.K., on May 5, 1959. He received the B.Sc. degree in physics from Imperial College of Science and Technology, U.K., the M.Phil. degree in space physics from Sheffield University, U.K., and the Ph.D. degree in electrical engineering from the University of Nottingham, U.K., in 1981, 1987, and 1990, respectively.

In 1990, he joined the Department of Electrical and Electronic Engineering, University of Nottingham as a Lecturer. His research interests are in electromagnetic compatibility, electrostatic precipitation, and the protection and simulation of power networks.